RSC Advances

PAPER

Cite this: *RSC Adv.*, 2015, **5**, 72716

Iron oxyhydroxide aerogels and xerogels by controlled hydrolysis of $FeCl_3 \cdot 6H_2O$ in organic solvents: stages of formation

I. Lázár,[a] A. Szilágyi,[a] G. Sáfrán,[b] Á. Szegedi,[c] S. Stichleutner[d] and K. Lázár*[d]

Received 4th June 2015
Accepted 21st August 2015

DOI: 10.1039/c5ra10606k

www.rsc.org/advances

Iron oxyhydroxide aerogels and xerogels were prepared by controlled hydrolysis of $FeCl_3 \cdot 6H_2O$ in organic solvents by using a limited amount of water or consuming solely water molecules available from the crystals. Ethanol, ethylene glycol, dimethyl sulfoxide (DMSO) and dimethyl formamide (DMFA) solvents were used, the hydrolysis was promoted with epichlorohydrin proton scavanger. High surface area aerogels were prepared by supercritical CO_2 extraction of solvents, surface area and pore distribution measurements were performed on them. Aerogel and xerogel samples were characterized by XRD, Mössbauer spectroscopy and HRTEM methods. The process of hydrolysis was followed by recording Mössbauer spectra of frozen reaction mixtures. Stepwise progress and appearance of transient components were detected in DMSO and DMFA solvents. Aerogel samples exhibit asymmetric spectra with low probability of Mössbauer effect in their as synthesized state. In contrast, frozen reaction mixtures, gels, dry xerogels and compressed aerogels display symmetric spectra with high probability of the Mössbauer resonance. XRD proves the dominant presence of 2-line ferrihydrite. HRTEM studies reveal 4–8 nm typical particle sizes with 0.21–1.0 nm characteristic lattice distances. Different types of coordination environments are distinguished for iron in the formed ferrihydrite nanoparticles due to structural features and imperfections.

Introduction

Syntheses and application of mesoporous transition metal oxides have attracted enhanced interest recently.[1] Among these, preparation of mesoporous iron oxide is also subject of various studies. It can be synthesized *e.g.* by hydrolysis of ethoxy-iron[2,3] or by sol–gel technique in inverse micelles.[1] Aerogels attract particular interest since they exhibit specific properties, *e.g.* their moderate stiffness is combined with very high specific surface area and low density.[4,5] They can be used as substances with special magnetic properties,[6–8] as catalysts[9,10] or as precursors of specific reagents (Al/Fe_2O_3)[11] or as heat insulators.[5] Furthermore, oxyhydroxide gels can also be used for water remediation.[12] Iron oxide and -oxyhydroxide xero- and aerogels have already been successfully synthesized in various laboratories by controlled hydrolysis. In a version of these processes only a limited amount of water is used. For instance, even the stoichiometric amount of crystalline water in $FeCl_3 \cdot 6H_2O$ might be sufficient. Ethanol (ET), ethylene glycol (EGLY), dimethyl sulfoxide (DMSO) and dimethyl formamide (DMFA) are often used. They have different solvation characteristics. Namely, glycol is chelating, both DMSO and DMFA are donor aprotic solvents, the latter has more basic character. Each of them may form stable complexes with iron or iron chloride as well.[13–18] Mixtures of water with organic solvents have also been tested for preparation of xero- and aerogels.

In this procedure, an important condition is the control of hydrolysis by addition of 1,2-epoxide, *e.g.* propylene oxide, which may eliminate the proton formed in the first step of hydrolysis of the hexaqua iron complex.[19] Propylene oxide can be replaced with epichlorohydrin for more convenient handling.[6,7,11,20] Successful application of 1,3 epoxides (*e.g.* trimethylene oxide) has also been reported.[21] The syntheses of xero- and aerogels are similar, except the very final step, the removal of solvents after gelation. For obtaining aerogels, supercritical CO_2 extraction should be applied[8,22] otherwise dense xerogels form.

Early stages of hydrolysis in aqueous media are well-known in detail.[23] First dimers are formed with hydroxo bridges in aqueous media (olation). A detailed study reports on existence of six types of dimeric species.[24] In non-aqueous media oxo bridges may form (oxolation), then network of condensed

[a]*Department of Inorganic Chemistry, University of Debrecen, Egyetem tér 1, 4010 Debrecen, Hungary*

[b]*Centre of Energy Research, MTA, MFA, Konkoly Thege M. 29-33, 1121 Budapest, Hungary*

[c]*Research Centre for Natural Sciences, MTA, IMEC, Magyar tudósok körútja 2, 1117 Budapest, Hungary*

[d]*Centre of Energy Research, MTA, EKBI, Konkoly Thege M. 29-33, 1121 Budapest, Hungary. E-mail: lazar.karoly@energia.mta.hu*

oxyhydroxide develops. Formation of complexes with solvent molecules may retard hydrolysis and enhance condensation.[20,25]

Products of hydrolysis can be identified from HRTEM studies by determining the values of lattice constants in the formed small particles. Formation of different oxyhydroxides (ferrihydrite,[26] goethite, α-FeO(OH), akageneite, β-FeO(OH), lepidocrocite, γ-FeO(OH)[27]) can be observed depending on the conditions.

Another frequently applied method is the X-ray diffractometry (XRD). Even the most poorly ordered structure, ferrihydrite can be also analysed.[8,20,22] Depending on the extent of the ordering, "2-line" and "6-line" ferrihydrites are distinguished.[27] More recent high energy X-ray scattering studies reveal that the observed signal depends on the size of the scattering domains.[26]

Mössbauer spectroscopy is also a convenient tool for studying iron compounds. This technique is used primarily to characterize solid substances. Various oxides, oxyhydroxides have been investigated in detail with the method.[28] Structure of crystalline molecules *e.g.* $FeCl_3 \cdot 6H_2O$ is well-known from XRD studies,[29] it can be compared with corresponding Mössbauer spectra.[30] Stable solid molecular complexes of iron formed with DMSO, DMFA have already been prepared and characterized with this technique, as well.[14,15] Very early stages of hydrolysis of iron were also followed by careful separation of products with dialysis and measurements after freeze-drying in solid state. Monomeric, dimeric and polymeric species were identified in characteristic spectra.[31] The process of hydrolysis can also be studied directly in frozen solutions, as described in detail in aqueous media.[32] Solvation in different aprotic solvents was also followed.[12,33] Xero- and aerogel end products were also characterized in several instances by the technique,[7,10,20] in particular details in ref. 34. Further on, the probability of the Mössbauer effect (*f*-factor) can also be extracted from the spectra and its value may supply additional information on the bonding conditions of various species.[29,35] Namely, the logarithm of the *f*-factor is inversely proportional to the product of the effective mass and the vibration frequency of the γ-emitting species.[36] Significant differences have been observed in the probability of the Mössbauer effect for xero- and aerogels, and a parameter, the Mössbauer effective thickness has also been introduced to describe the efficiency of the absorption/emission process in the lattice.[34] Although usually one type of iron site exists in the oxyhydroxides (exception β-FeOOH)[24] superposition of three components was necessary for the acceptable description of spectra of xero- and aerogels.[34]

It can be noticed however that the first stages of hydrolysis of iron in non-aqueous, organic media have not been studied in detail yet. Therefore the aim of the present communication is laid primarily on this aspect. First stages of hydrolysis are supposed to proceed in the same way for both the aerogels and xerogels prior to completion of gel formation. Thus, studies both on aerogels and on xerogels are described in our present report.

First, preparation and characterization of aerogels and xerogels are described. Hydrolysis of $FeCl_3 \cdot 6H_2O$ in DMSO/water and ET/water solutions, and in anhydrous DMSO, DMFA and EGLY solvents was performed by using epichlorohydrin as proton scavanger. Products are characterized with adsorption measurements, XRD, HRTEM and Mössbauer methods. Main emphasis is laid on the study of the first stages of gel formation by Mössbauer spectroscopy of frozen reaction mixtures.

Experimental

Processes and samples

Hydrolysis of $FeCl_3 \cdot 6H_2O$ was performed in two types of experiments, either in DMSO–water and in ethanol–water mixtures or without additional water, in pure DMSO, DMFA, and EGLY solvents. Epichlorohydrin was used as a proton scavanger. The used chemicals were obtained from Sigma-Aldrich. First, iron chloride was completely dissolved, then epichlorohydrin (C_3H_5OCl) was added to the clear solution in portions.

The molar ratio of components in the DMSO–water experiments was Fe : DMSO : H_2O : C_3H_5OCl = 1 : 30 : 36 : 8.3. Aerogels were also prepared from these samples by supercritical extraction of solvents. First the DMSO and water media was exchanged for methanol solvent, then methanol was exchanged gradually to dry acetone. The sample was placed to an autoclave, then liquid CO_2 was introduced at *ca.* 50 bar pressure. The acetone solvent was removed as a separate phase. Then the temperature was increased to 80 °C, where CO_2 transforms to supercritical state. After 3 h the CO_2 was slowly decompressed and cooled, thereby dry monolithic aerogel was obtained.

In the second type of experiments (under anhydrous conditions) 2.9 mmol of $FeCl_3 \cdot 6H_2O$ was dissolved in 6 ml of solvent (DMSO or DMFA or EGLY) and after dissolution of the salt 1.6 ml of epichlorohydrin was dropwise added with stirring. To follow the progress of hydrolysis *ca.* 1 ml samples were taken after different elapsed time intervals, even before gelation has been completed. These samples were immediately frozen by immersion to liquid nitrogen. Gelation has taken place in the remaining portions of the mixtures after 4–6 hours. These gels were stored for several days at room temperature. Primary solvents were removed by repeated extraction with ethanol, then xerogels formed upon evaporation of the ethanol at room temperature. The drying process resulted in *ca.* 50-fold decrease in the volume of the original gel.

In specification of samples A and X prefixes are used for aerogels and xerogels, respectively. The next label identifies the solvent media. For example A-(DMSO + H_2O) denotes an aerogel sample prepared in DMSO + water mixture, or X-DMFA stands for a xerogel prepared in non-aqueous DMFA media.

Characterization of samples

Specific surface area/BET and pore size distribution measurements were performed on aerogel samples with a Quantachrome Nova 2200e surface area and porosity analyzer using nitrogen gas adsorbate (Quantachrome Instruments, Boynton Beach, FL, USA) at 77 K temperature. Prior the measurement samples were outgassed at 50 °C in vacuum for 3 hours. In addition, sample A-(DMSO + H_2O) was outgassed at higher temperatures (150 and 250 °C) as well.

X-ray powder diffraction patterns were recorded by a Philips PW 1810/3710 diffractometer with Bragg–Brentano parafocusing geometry applying monochromatized CuK_α ($\lambda = 0.15418$ nm) radiation (40 kV, 35 mA) and proportional counter. Counts were collected at 0.02 degree two theta steps for 1 s.

Combustion analysis was applied to determine the elemental composition of some aerogel samples with a Vario MICRO Cube CHNS analyser (Elementar Analysensysteme GmbH, Hanau, Germany). The samples are incinerated at temperatures exceeding 1000 °C, the products of oxidation are analysed.

Scanning electron microscopic (SEM) images were recorded on a Hitachi S-4300 instrument (Hitachi Ltd., Tokyo, Japan) equipped with a Bruker energy dispersive X-ray spectroscope (Bruker Corporation, Billerica, MA, USA). The monolithic aerogel samples of approximately 2–4 mm sizes were embedded in a low melting point alloy (Wood's metal) to decrease the possibility of accumulation of electric charge in the highly insulating aerogel samples. All fresh fracture surfaces were covered by a sputtered gold conductive layer. Typically, a 10–15 kV accelerating voltage was used for taking high resolution pictures.

TEM and HRTEM measurements for aero- and xerogel samples were performed by using either a Philips CM20, 200 kV conventional Transmission Electron Microscope (TEM, point resolution: 0.24 nm) or a JEOL 3010 300 kV High Resolution TEM (HRTEM – point resolution: 0.17 nm) equipped with an Electron Energy Loss Spectrometer (EELS) and a GATAN Tridiem Image Filter (GIF). Selected Area Electron Diffraction (SAED) patterns could be obtained with the former instrument, whereas characteristic lattice distance values were determined from certain good quality images by Fast Fourier Transformation (FFT) process in the latter apparatus. Qualitative analysis for chlorine was also performed with EELS elemental mapping.

Mössbauer spectra were obtained both on the frozen solutions and on the final products as well. Frozen solutions were measured in *ca.* 1 ml volumes (*ca.* 2.5 mm thick disks with 2 cm diameter) at 77 K. In order to prove that primarily iron oxyhydroxides are formed one aerogel sample was evacuated at 260 °C in the *in situ* Mössbauer cell. Both the 77 K measurements of the frozen samples and the mentioned evacuation were performed in the *in situ* cell described in ref. 37. As prepared dry aerogel samples were also measured. In some instances they were compressed to obtain better quality spectra (30 MPa cm^{-2}). The used spectrometer is a KFKI equipment, the drive was operating in constant acceleration mode. For recording these spectra 0.5 GBq $^{57}Co/Rh$ source was used. Spectra were decomposed to Lorentzian lines, no constraints were used, the accuracy of the positional data is *ca.* ± 0.03 mm s^{-1}. The isomer shift values are related to alpha-iron. Temperature dependence of the shape of Mössbauer spectra was also investigated on a partly dried sample (*ca.* 50 wt% glycol solvent remained). This series was recorded in another apparatus, in a vertical cryostat with a WISSEL drive operating in sinusoidal mode.[38] There is no temperature shift in the observed isomer shift value in the latter case since both the sample and the Mössbauer source are at the same temperature (in contrast to the previous KFKI assembly).

Results

Aerogel samples

Aerogel samples were prepared first. Their density was *ca.* 0.1 g cm^{-3} after extraction with the supercritical CO_2. A typical photograph of the A-(ET + H_2O) sample is shown in Fig. 1.

Adsorption measurements

Sorption isotherms were measured on the A-(DMSO + H_2O) and A-DMSO samples. The former sample was outgassed at different temperatures in order to study the stability and the extent of possible textural changes upon moderate heat treatments. For illustration, adsorption and desorption isotherms of the sample outgassed at 50 and 250 °C are shown in Fig. 2.

The obtained isotherms are of type II (IUPAC classification) with H3 type hysteresis loop, typical for oxides with aggregated particles. BET surface area, principal constants of BET equation,[39] pore volume values, and pore size distributions were also determined (Table 1).

The obtained specific surface area and pore volume values are close to those reported in ref. 8, whereas the pore size distributions in our samples are more narrow.

Fig. 1 Photograph of a typical aerogel sample A-(ET + H_2O) compared to a cm scale.

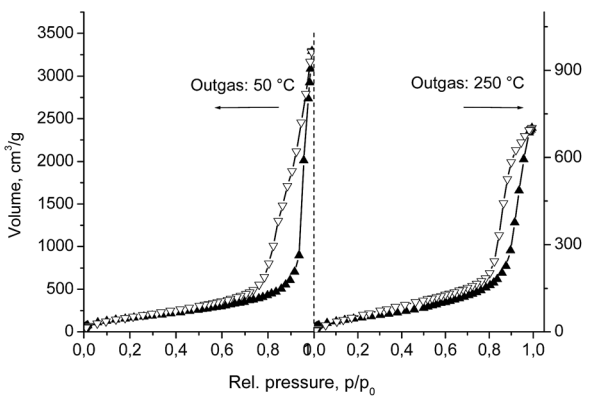

Fig. 2 Adsorption–desorption isotherms for the A-(DMSO + H_2O) sample outgassed at 50 °C (left) and 250 °C (right). Adsorption: ▲, desorption: ▽.

Table 1 Basic sorption data obtained on aerogel samples (T_{out}: temperature of outgassing, Sp. area: specific surface area, B Eq slope and B Eq C const: slope and C constant of BET equation, respectively, Por. vol.: pore volume, Max. diam., location of maximum in the pore size diameter distribution, calculated from the desorption branch)

Sample	T_{out} °C	Sp. area $m^2\ g^{-1}$	B Eq slope	B Eq C	Por. vol $cm^3\ g^{-1}$	Max. diam. nm
DMSO + H_2O	50	615	5.52	39.0	5.33	12.8
DMSO + H_2O	150	471	7.20	39.3	3.9	16.8
DMSO + H_2O-1	250	179	18.6	25.8	1.12	14.5
DMSO + H_2O-2	250	191	17.45	24.2	1.17	14.6
DMSO	50	671	5.05	38.1	3.7	17.0

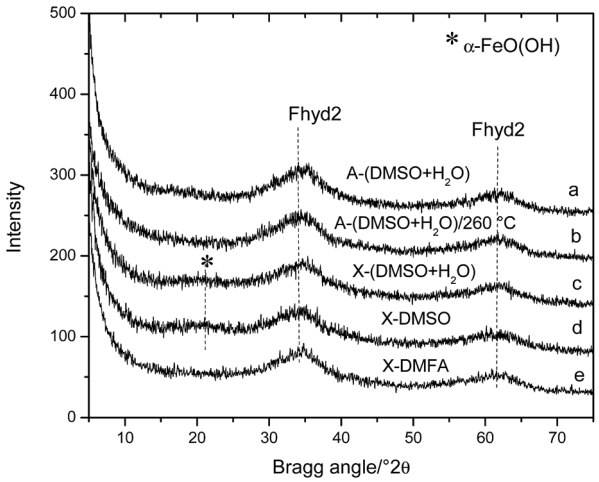

Fig. 3 X-ray diffractograms of various aerogel and xerogel samples. For comparison locations of the peaks of 2-line ferrihydrite and α-FeOOH (goethite) are also marked.

Comparison of data obtained on sample A-(DMSO + H_2O) outgassed at different temperatures reveal that significant textural changes take place in the aerogel above 150 °C. In spite of the textural changes the high surface area and the maximum at *ca.* 15 nm pore diameter is preserved after 250 °C treatment, *i.e.* basic characteristics of aerogels are sustained.

X-ray diffraction patterns were recorded on A-(DMSO + H_2O) sample after drying and after a further evacuation performed at 260 °C (Fig. 3a and b). The diffractograms exhibit broadened lines characteristic to small particles with sizes of domains of coherent reflection with 3–5 nm. The two broad peaks are characteristic of the 2-line ferrihydrite (Fhyd2).

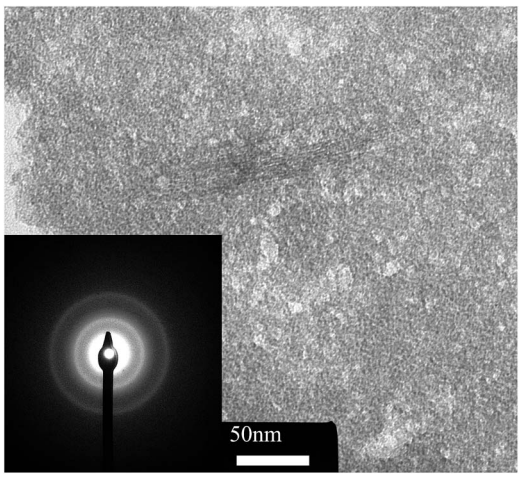

Fig. 4 TEM micrograph of the A-(DMSO + H_2O) sample with SAED insert of the corresponding region.

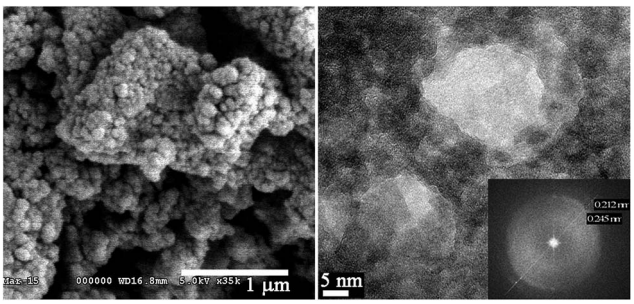

Fig. 5 SEM (left) and HRTEM (right) images of A-DMSO sample, the latter with FFT insert, displaying 0.212 and 0.245 nm characteristic lattice distance values.

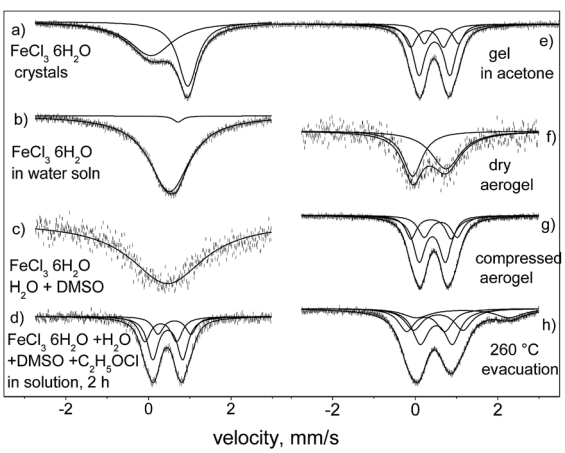

Fig. 6 Stages of aerogel formation in DMSO-water media shown in 77 K Mössbauer spectra. Crystalline solid $FeCl_3 \cdot 6H_2O$ (top left, a), $FeCl_3 \cdot 6H_2O$ in aqueous solution (b), $FeCl_3 \cdot 6H_2O$ + water + DMSO (c), $FeCl_3 \cdot 6H_2O$ + water + DMSO + epichlorohydrin, 2 h after mixing, still in liquid state (d), after gelation, washed in acetone (top right, e), dry aerogel after supercritical CO_2 extraction (f), after compressing the aerogel (g), and after evacuation at 260 °C (h).

SEM, TEM and HRTEM measurements revealed also the porous structure of the assembled iron oxyhydroxide nanoparticles. For illustration TEM micrograph of the A-(DMSO + H_2O) sample and SEM and HRTEM images of A-DMSO sample are shown in Fig. 4 and 5 respectively.

The HRTEM image reveals that the aerogel is assembled from nanocrystallites of *ca.* 5 nm diameter, with 0.212 and 0.245 nm characteristic lattice distance values.

Further, the A-(ET + water) sample was also characterized by SEM and HRTEM, similar lattice constant values can be extracted by FFT analysis (0.206, 0.251 and 0.297 nm) from these images as well.

Mössbauer spectroscopy can be applied to follow the whole process of dissolution, gelation, drying and even effects of further heat treatments can be studied. Spectra corresponding to stages of preparation of A-(DMSO + H_2O) sample are presented in Fig. 6.

Spectra, shown in the left side of Fig. 6 were obtained on frozen samples containing similar amounts of iron. Surprisingly, despite of the solid (frozen) state the probability of Mössbauer effect decreased significantly in the DMSO + water mixture. It is also worth noticing that in the very early stage, even prior to the gel formation almost the same parameters can be obtained from the Mössbauer spectrum (Fig. 6d) than after gelation (Fig. 6e), or after extraction with supercritical CO_2 (Fig. 6g). After gelation the probability of Mössbauer effect increased again.

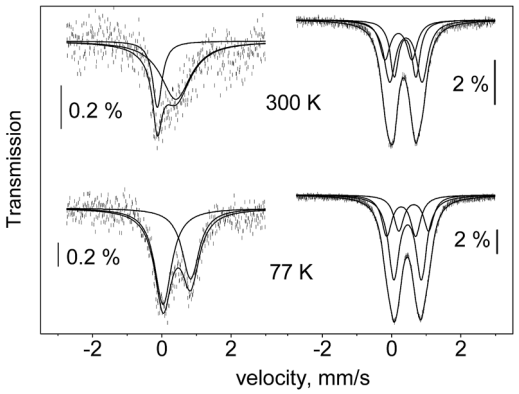

Fig. 7 Comparison of 300 and 77 K Mössbauer spectra of the aerogel sample prepared in anhydrous DMSO media in as received aerogel form (left) and after compression (right).

Good quality fits can be obtained by spectral decomposition to three doublets (Table 2). It should be noted that the parameters are rather similar either gels or solid (dried and compressed) aerogels are considered (data extracted from spectra of further samples are also shown in Table 2 for comparison).

The combination of high porosity with loose structure in aerogels can also be demonstrated by comparing the Mössbauer spectra of the original light aerogels with those obtained after compression of samples. Corresponding 300 and 77 K spectra for A-DMSO sample are shown in Fig. 7. It is clearly seen that the response factor dramatically increases by the compression (100 MPa). More surprisingly not only the probability of the effect but the shape of spectra are also influenced. The phenomenon is general, it can be observed on all the studied aerogel samples (Table 3).

Thermal treatments were also carried out on the aerogel samples in order to study the stability and eventual transformations of oxyhydroxides.

Mild thermal treatment, namely evacuation at 260 °C was performed to distinguish whether oxide or oxyhydroxides are formed during gelation and drying. Sorption measurements on

Table 2 Data extracted from 77 K Mössbauer spectra (δ: isomer shift, Δ: quadrupole splitting, RI: relative spectral contribution)

Sample media/ condition	Component	δ mm s^{-1}	Δ mm s^{-1}	RI %
A-(DMSO + H_2O)	Fe^{3+}(1)	0.30	0.79	30
Gel in acetone	Fe^{3+}(2)	0.47	0.74	47
Frozen	Fe^{3+}(3)	0.63	0.81	24
A-(DMSO + H_2O)	Fe^{3+}(1)	0.28	0.80	22
Dry aerogel	Fe^{3+}(2)	0.46	0.74	54
Compressed	Fe^{3+}(3)	0.64	0.80	24
A-(ET + H_2O)	Fe^{3+}(1)	0.21	0.96	3
Dry aerogel	Fe^{3+}(2-1)	0.47	0.61	55
Compressed	Fe^{3+}(2-2)	0.47	0.96	42
X-(DMSO + H_2O)	Fe^{3+}(1)	0.30	0.77	32
Reaction mixture	Fe^{3+}(2)	0.47	0.72	45
Frozen gel	Fe^{3+}(3)	0.63	0.79	22
X-(DMSO + H_2O)	Fe^{3+}(1)	0.26	0.77	36
Dried gel	Fe^{3+}(2)	0.46	0.75	29
	Fe^{3+}(3)	0.65	0.80	35
X-DMSO	Fe^{3+}(1)	0.29	0.82	30
Dried gel	Fe^{3+}(2)	0.52	0.73	58
	Fe^{3+}(3)	0.56	1.11	12
X-EGLY	Fe^{3+}(1)	0.31	0.83	23
Reaction mixture	Fe^{3+}(2)	0.47	0.77	49
Frozen gel	Fe^{3+}(3)	0.64	0.81	28
X-EGLY	Fe^{3+}(1)	0.28	0.85	5
Dried gel	Fe^{3+}(2-1)	0.49	0.58	43
	Fe^{3+}(2-2)	0.50	0.94	52
X-DMFA	Fe^{3+}(2-1)	0.46	0.60	71
Reaction mixture	Fe^{3+}(2-2)	0.46	0.96	26
Frozen gel	Fe^{3+}(2-3)	0.47	1.32	12
X-DMFA	Fe^{3+}(1)	0.26	0.79	24
Dried gel	Fe^{3+}(2)	0.50	0.67	55
	Fe^{3+}(3)	0.53	1.03	20

Table 3 Comparison of the relative spectral area values of pristine aerogel samples and after compression extracted from 77 and 300 K spectra ($R_{77/300}$ is the ratio of the 77 and 300 *K* values)

Sample	Temp.	Aerogel	$R_{77/300}$	Compr.	$R_{77/300}$
A-(ET + H_2O)	77 K	0.149	1.243	2.478	3.404
	300 K	0.120		0.728	
A-(DMSO + H_2O)	77 K	0.187	2.764	2.391	2.113
	300 K	0.068		1.131	
A-DMSO	77 K	0.183	2.347	1.722	2.650
	300 K	0.078		0.650	

Table 4 Approximate nominal molar compositions of aerogels determined from combustion measurements

Sample/solvent	Fe_2O_3	H_2O	DMSO	C_3H_5OCl
A-(DMSO + H_2O) (1)	1	1.24	0.006	0.53
A-(DMSO + H_2O) (2)	1	1.0	0.017	0.72
A-DMSO	1	1.0	0.031	0.61
A-(ET + H_2O)	1	1.5	0.0	0.63

A-(DMSO + H_2O) sample reveal a significant decrease in the specific surface area and pore volume values (Table 1). However, the structure has not been modified significantly, X-ray diffractograms for the same non-heated and heated samples are similar (Fig. 3a and b). Evacuation or moderate heating of oxyhydroxides in inert atmospheres may result in formation of mixed Fe^{2+}/Fe^{3+} oxides (*e.g.* magnetite). Indeed, Fe^{2+} appears in the corresponding Mössbauer spectrum in accordance with the expectation (Fig. 6h). Furthermore, this sample can be magnetized with a permanent magnet, too.

More severe combustion treatment was also applied to access information on the approximate composition of samples, high chlorine contents were obtained (Fe : Cl ≈ 1 : 0.3, Table 4).

Xerogel samples

Adsorption measurements have not been performed on xerogel samples since they are *ca.* 50-fold denser than their aerogel counterparts.

X-ray diffractograms were recorded on certain xerogel samples (Fig. 3c–e). Patterns are similar to those obtained on aerogels. The broad peaks are primarily originated from 3–5 nm 2-line ferrihydrite particles. Presence of goethite in minor amounts can also be detected in samples prepared in DMSO media (Fig. 3c and d).

SEM and HRTEM studies provided similar images to those found on aerogel samples. Namely, xerogel samples are composed from small nanoparticles of iron oxyhydroxides of *ca.* 5 nm size in average. This indicates that first stages of formation of aerogels and xerogels are similar.

As an illustration, HRTEM images recorded on the X-EGLY sample are presented in Fig. 8. EELS elemental mapping was performed at 200 eV energy loss, characteristic to chlorine. The bright contrast image in bottom right indicates the presence of chlorine in significant amount (in correspondence with data presented in Table 4 for aerogel samples).

Other xerogels were also studied by HRTEM, and corresponding characteristic lattice constant values were obtained. For X-DMFA 0.208, 0.253 and 0.305 nm values were extracted by FFT analysis.

Mössbauer studies on xerogels provided similar δ and Δ values to those obtained on frozen reaction mixtures and on aerogels (see Table 2). The dense structure of the products is reflected in the characteristic high response factors of the dried samples.

Further on, a particular feature, stepwise development of the final structure can be illustrated in the xerogels. Namely, deviation from the expected regular temperature dependence of the

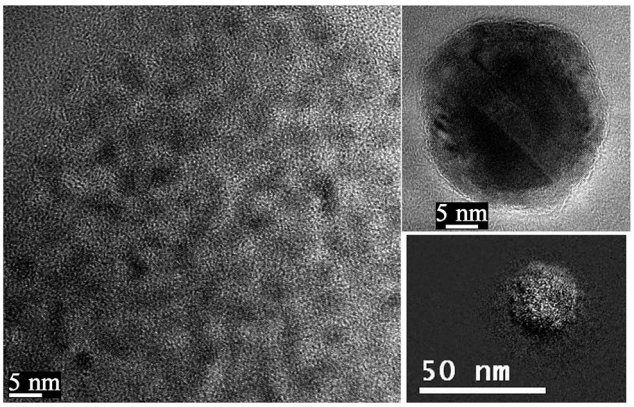

Fig. 8 HRTEM images of the X-EGLY sample. Part of an extended region (left), separate particle (right top), bright contrast chlorine EELS elemental map on the same particle (right bottom – note the different magnification on the right side).

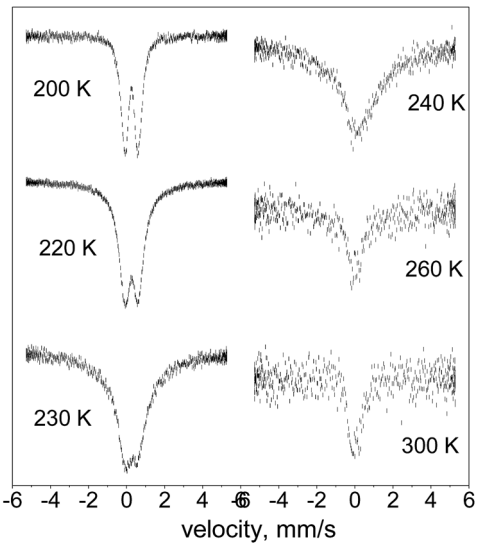

Fig. 9 Temperature dependence of Mössbauer spectra on an X-GLY sample recorded after incomplete extraction with ethanol (containing still *ca.* 50 wt% glycol).

probability of the Mössbauer effect can be observed on samples from which the original solvent has not been removed completely. Extraction of glycol with ethanol was incomplete in preparation of a X-GLY sample, *ca.* 2–3 glycol molecules per iron atoms were still present after removal of ethanol with drying. On this sample only a weak signal could be detected at room temperature. To clarify further details a series of spectra was collected on this sample in dependence of temperature in the 80–300 K region (Fig. 9). Spectra were collected at 80, 120 and 160 K as well (not shown), they exhibit the same shape as the 200 K one. The relative spectral contribution (proportional to the *f*-factor) can also be calculated and plotted against temperature (Fig. 10).

The curve exhibits the expected shape of temperature dependence in the 80–200 K region which can be described with a single Debye temperature value. In contrast, there is an expressed breakdown at higher temperatures, starting from 220 K.

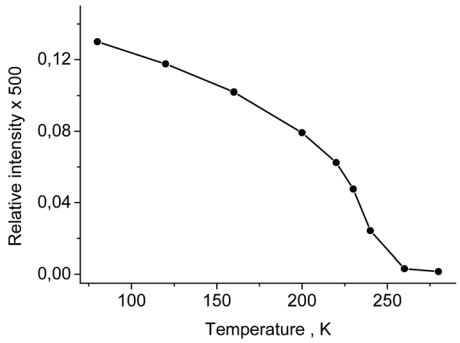

Fig. 10 Temperature dependence of the relative spectral area values of a X-GLY sample after incomplete extraction with ethanol (based on spectra shown in Fig. 9).

Kinetics of gel formation

Depending on the solvent media (EGLY, DMSO and DMFA) significant differences are revealed in the early stages of gel formation.

In ethylene glycol formation of the primary oxyhydroxide particles is fast – within 10 minutes their final structure develops. The same data can be extracted from the Mössbauer spectrum of the sample frozen after 10 minutes of mixing of the components and from the spectrum of the final state after washing and drying (see Table 2 and Fig. 11).

The hydrolysis is slower in DMSO, Mössbauer spectra of intermediate stages can be intercepted. The main component in the spectrum of the reaction mixture recorded after 5 minutes of mixing exhibits high quadrupole splitting ($\Delta \sim 1.7$ mm s^{-1}). This value exceeds significantly the $0.6 < \Delta < 0.8$ mm s^{-1} values, characteristic for the stabilized products. These components became dominant only after *ca.* 30 minutes of mixing the components in DMSO (Fig. 12 and Table 5).

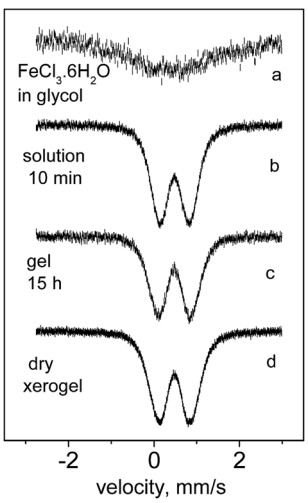

Fig. 11 77 K Mössbauer spectra recorded during the stages of formation of X-GLY sample. $FeCl_3 \cdot 6H_2O$ in ethylene glycol, frozen (a), reaction mixture, 10 minutes after addition of epichlorohydrin (b), in gel form (c) and after drying, as X-GLY (d).

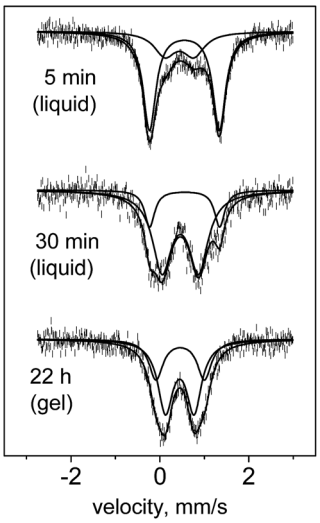

Fig. 12 77 K Mössbauer spectra obtained at different intervals after addition of figure epichlorohydrin to $FeCl_3 \cdot 6H_2O$ + DMSO solution.

Table 5 Mössbauer parameters extracted from the fits of 77 K spectra in stages of formation of X-DMSO gel (δ: isomer shift, Δ: quadrupole splitting, RI: relative spectral contribution)

Time	Comp.	δ mm s^{-1}	Δ mm s^{-1}	RI %
5 min	Fe^{3+}(2)	0.44	0.65	28
	Fe^{3+}(tr)[a]	0.55	1.57	72
30 min	Fe^{3+}(2)	0.46	0.82	80
	Fe^{3+}(tr)[a]	0.56	1.57	20
22 h	Fe^{3+}(2-1)	0.45	0.64	65
	Fe^{3+}(2-2)	0.46	1.09	35

[a] Fe^{3+}(tr) stands for transient species.

In DMFA media the process of hydrolysis proceeds apparently more slowly as compared to DMSO. The stages are more distinct, as could be deduced from corresponding 77 K Mössbauer spectra shown in Fig. 13 (with corresponding data in Table 6).

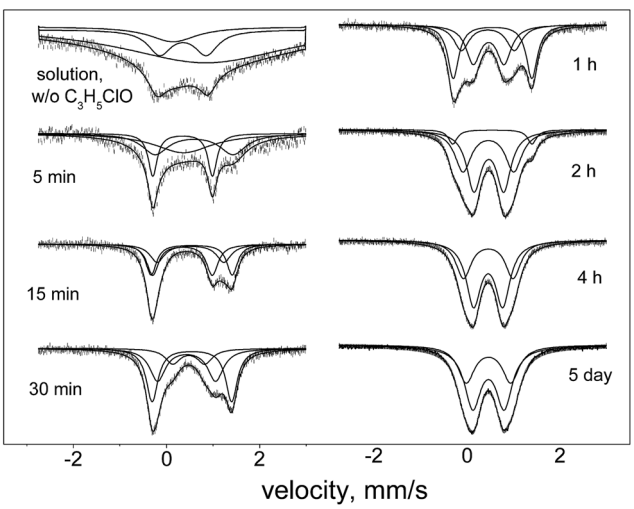

Fig. 13 Mössbauer spectra displaying stages of formation of X-DMFA gel, after different intervals of addition of epichlorohydrin.

Table 6 Data obtained from decomposition of 77 K Mössbauer spectra of frozen $FeCl_3 \cdot 6H_2O$ + DMFA + C_3H_5OCl, solutions recorded after different intervals after addition of epichlorohydrin (δ, isomer shift, Δ quadrupole splitting, FWHM, line width, RI, relative spectral contribution)

	δ mm s^{-1}	Δ mm s^{-1}	FWHM mm s^{-1}	RI %
DMFA solution				
Fe^{3+}(singlet)	0.31	—	2.71	89
Fe^{3+}(soln1)	0.36	0.64	0.22	3
Fe^{3+}(soln2)	0.36	1.18	0.30	8
5 min				
Fe^{3+}(singlet)	0.35	—	1.51	34
Fe^{3+}(t-1)[a]	0.35	1.28	0.24	26
Fe^{3+}(t-2)[a]	0.60	1.66	0.77	39
15 min				
Fe^{3+}(t-1)	0.34	1.31	0.32	43
Fe^{3+}(t-2)	0.55	1.65	0.36	57
30 min				
Fe^{3+}(t-1)	0.36	1.39	0.31	23
Fe^{3+}(t-2)	0.57	1.64	0.34	53
Fe^{3+}(3)	0.46	0.76	0.44	24
1 h				
Fe^{3+}(t-2)	0.55	1.69	0.29	38
Fe^{3+}(2-1)	0.46	0.66	0.38	35
Fe^{3+}(2-2)	0.45	1.14	0.42	27
2 h				
Fe^{3+}(t-2)	0.54	1.70	0.23	8
Fe^{3+}(2-1)	0.47	0.64	0.38	53
Fe^{3+}(2-2)	0.46	1.10	0.42	39
4 h				
Fe^{3+}(2-1)	0.45	0.63	0.38	62
Fe^{3+}(2-2)	0.46	1.07	0.40	38
5 day				
Fe^{3+}(2-1)	0.46	0.63	0.42	63
Fe^{3+}(2-2)	0.47	1.07	0.42	37

[a] Fe^{3+}(t-1) and Fe^{3+}(t-2) stand for the transient components.

The first spectrum was recorded prior to the addition of epichlorohydrin (top left). The process of gelation commences *ca.* within 4 h. In correspondence, all the spectra are obtained on frozen liquid samples, except the very last spectrum, which was recorded on frozen gel (Fig. 13, right bottom).

Appearance and relative contributions of various components can also be plotted in dependence of time (Fig. 14). It is seen that Fe^{3+}(singlet), Fe^{3+}(t-1) and Fe^{3+}(t-2) are transient species, they are transformed to the stable Fe^{3+}(2-1) and Fe^{3+}(2-2).

Further important information can also be extracted from the Mössbauer spectra. Namely, the response factors, *i.e.* the probabilities of Mössbauer effect are distinctly different in dependence of time (Fig. 15). An expressed (almost five-fold) increase can be revealed in the values of the average relative spectral area. In other words, the sums of response factors for components Fe^{3+}(singlet), Fe^{3+}(t-1) and Fe^{3+}(t-2) are significantly smaller than response factors of components Fe^{3+}(2-1) and Fe^{3+}(2-2) in Table 6 and Fig. 14.

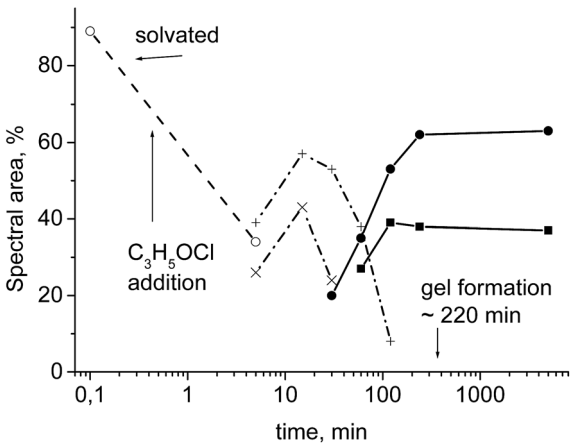

Fig. 14 Kinetics of oligomerisation: proportions of components appearing in the spectra of Fig. 13. - o - Fe^{3+}(singlet), - x - Fe^{3+}(t-1), - + - Fe^{3+}(t-2), - ● - Fe^{3+}(2-1), - ■ - Fe^{3+}(2-2).

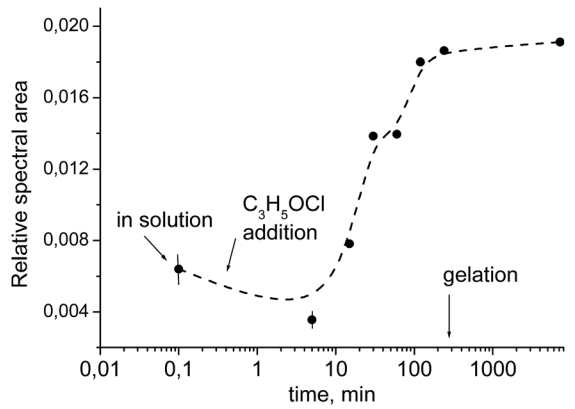

Fig. 15 Time dependence of the average relative spectral area (spectral area related to the "full area", *i.e.* intensity of base line multiplied by channel number). Note the logarithmic time scale.

Discussion

Stages of hydrolysis – early products and kinetics

New insights were achieved in the study of the early steps of formation of iron oxyhydroxide gels by using Mössbauer spectroscopy of frozen solutions in organic media. Stages of hydrolysis, replacement of ligands around iron from the initial $[FeCl_2(H_2O)_4]^+$ could be followed. In particular, the spectrum of the starting crystalline $FeCl_3 \cdot 6H_2O$ is a characteristic asymmetric doublet, originated both from relaxation and Karyagin–Goldanskii effects.[30] Dissolution in water results in the destruction of the crystal lattice, the mentioned effects vanish, a single broad line is seen in the spectrum of the frozen aqueous solution. This spectrum is similar to those found in freeze-dried samples and is attributed to monomeric species.[31] A rather good response factor is observed – the structure of frozen water is rigid – hydrogen bridges are stabilizing it (Fig. 6a and b). In contrast, the probability of the effect is decreased significantly in the frozen solution at the $FeCl_3$: DMSO : H_2O = 1 : 30 : 36

molar ratio, showing that the structure of frozen DMSO + water solution is less rigid than in ice (Fig. 6c). At the actual molar ratios of components certain exchange of H_2O ligands to DMSO around iron can be expected. The $[FeCl_2(H_2O)_{4-x}(DMSO)_x]^+ \rightarrow [FeCl_2(OH)(H_2O)_{3-x}(DMSO)_x]$ hydrolysis proceeds by addition of epichlorohydrin, since the formed protons are consumed for protonation of epoxy groups. Chloride ions can also be consumed for opening the epoxy bridges in the protonated epichlorohydrin as described in ref. 19. In the further stage olation takes place, di- and oligomers may form, and at the end of the process a network of oxyhydroxide particles is assembled. Hydrolysis and agglomeration are probably fast in water containing media, iron oxyhydroxide agglomerates form but they probably cannot grow to large size as a result of hindered particle motion due to presence of DMSO. The oxyhydroxide particles in the gel are stacked and fixed as is shown in the TEM image of Fig. 4.

Kinetics of hydrolysis is significantly slower in non-aqueous media when only six water molecules per iron are available from the starting $FeCl_3 \cdot 6H_2O$ crystals. Condensation is preferred when complexes can be formed with the solvent molecules compared to fast hydrolysis.[25] It was even possible to follow the different subsequent stages of hydrolysis in DMFA which is the strongest complexing molecule among the used aprotic solvents. Various stages of the process can be followed in Fig. 13–15. The $[2FeCl_3(DMFA)_3(H_2O)_2]$ complex is rather stable.[16,17] In the solution probably this complex molecule is prevailing. Upon addition of epichlorohydrin the hydrolysis commences. The axial symmetry around iron can be distorted, oligomerization may start. In accordance, transient (5, 15, 30 and 60 min) spectra are dominated with large quadrupole splitting components. It is worth to compare the number and parameters of species shown in Fig. 13 and 14 and listed in Table 6 with those found and identified in a pure aqueous phase. In aqueous phase three early products (with molecular weights less than 500) were identified: monomeric (broad singlet), dimeric (with a characteristic doublet, $\Delta \sim 1.2$ mm s^{-1}) and polymeric (doublet, $\Delta \sim 0.6$–0.8 mm s^{-1}, observed at 300 K).[31] In our case at hydrolysis in DMFA five components are clearly present, one of them exhibits a rather large quadrupole splitting ($\Delta \sim 1.7$ mm s^{-1} – Table 6). The larger number of participating transient components and the appearance of a particular component with large quadrupole splitting value clearly attests that not only aqua/hydroxo but mixed aqua/hydroxo/DMFA (/chloro) complexes are involved in the hydrolysis.

All these transient spectra are obtained on liquid samples frozen before gelation could commence. A further proof for the propagation of chain growth and network formation is also reflected in the progressive increase of the response factor of the Mössbauer effect during the ageing (Fig. 15). The significant, *ca.* five-fold increase in the *f*-factor is probably related both to the increase of the size of the involved species, and also to a simultaneous hardening, reflected in the increase of frequency of lattice vibrations.[36] Meanwhile, at the end of the process stable and symmetric octahedral environment composed of oxygen atoms around iron is constructed, the quadrupole splitting drops to $\Delta_{Fe^{3+}(3)} \sim 0.6$ mm s^{-1} and $\Delta_{Fe^{3+}(4)} \sim 1.07$ mm s^{-1} values, which are characteristic already for the formed polymeric species and oxyhydroxides.[31,34]

Aggregation of particles – variations of the f factors and change in the shape of spectra

The structure of obtained aerogels is rigid when supercritical extraction is used to remove the solvent media (Fig. 1). However, the microscopic structure is rather loose (Fig. 2). This is clearly demonstrated by comparing the spectra of pristine aerogels with those after compression (Fig. 7, Table 3). Similar observation is reported by comparing iron oxide aero- and xerogels, namely, 10–20-fold increase is reported in the Mössbauer effective thickness parameter (*i.e.* the same amount of iron in the sample gives 10–20 times larger response in xerogels than in aerogels[34]). In our case, a moderate compression of aerogels results in a *ca.* six-fold increase of the Mössbauer effect. Similarly to the previous instance this observation can probably be related to the change of the mass involved in the emission/absorption of γ-quanta, and to the change of vibration conditions of the lattice.[36] The effect of compression on the intensity of components in case of ^{119}Sn Mössbauer spectra of small particles is discussed in more detail in ref. 40.

It is important to note that not only the probability of the Mössbauer effect but the shape of spectra has also changed upon compression. Aerogels in their loose as received state display asymmetric spectra (see *e.g.* Fig. 7, left), and the asymmetry is more prevailing at higher temperatures. Similar change in the shape of spectra was reported in case of ferric hemin, the phenomenon was attributed to temperature dependent spin–spin relaxation times.[41] The effect of compression is also in accordance with this interpretation: particles get to close contact with each other, the spin–spin relaxation becomes much faster, the conventional symmetric shape of the doublet is restored.

Formation of xerogels probably has not been completed fully while a small portion of the original solvents is present in the structure after incomplete removal with ethanol. This is clearly illustrated in the case of one of the samples prepared in glycol media, when the final product contained *ca.* 50 wt% glycol. By physical appearance this sample is a rigid solid substance. Fig. 9 displays the change of the shape of spectra in dependence of the temperature, and Fig. 10 shows the temperature dependence of the response factor. In Fig. 9 the characteristic doublet starts to broaden at 220 K, and is smeared at 250 K. In correspondence, the temperature dependence of the response factor, which is proportional to the relative spectra area (shown in Fig. 10), exhibits a similar transition. In the 80–200 K region the regular Debye–Waller temperature dependence is followed, which can be described with a *ca.* $\Theta_D \approx 180$ K.[35] At higher temperatures (225–250 K) a significant drop appears, distinctly deviating from the expected shape. Thus, upon raising the temperature in this range a significant part of the bonds was released, only short oligomers participate in the resonance effect, instead of an extended network of tightly bound species. It can be mentioned that a similar behaviour is reported for $[Fe(DMSO)_5Cl]^{2+}$ cation,

a significant drop in the response factor is described in the 300–320 K region. The irregular behaviour of the DMSO complex is attributed to a structural phase transition.[14] The explanation of the irregular behaviour in our case can be different and more simple. Namely, the phenomenon can probably be connected to the gradual softening of the bonds with the interparticle glycol molecules (~melting) starting at 220 K. For comparison, it should be added that the sample after complete removal of glycol with ethanol and drying afterwards does not show this feature, it displays the expected doublet with high response factor at 300 K.

Further on it should also be mentioned that the formed particles are isolated from the point of view of magnetic coupling as well in our xero- and aerogel samples. For instance ferrihydrite samples composed of particles with 2–5 nm diameter exhibit resolved magnetic sextet at 80 K.[7,42] In contrast, in spite of the same particle size region this feature does not appear in our samples.

Final products of hydrolysis and their conversions at modest temperatures

Final products of hydrolysis carried out at ambient temperatures usually are oxyhydroxides (not oxides). It has been proven in our case as well.

At the first approach formation of all of the possible four types can be considered (ferrihydrite, and α-, β-, γ-oxyhydroxides). Depending on the rate of hydrolysis various structures may be stabilized. Rapid hydrolysis under ambient conditions favours formation of ferrihydrite,[31] slower hydrolysis and elevated temperatures (80–100 °C) may result in the formation of more ordered structures.[24,25,43] Several publications describe Mössbauer spectra of ferrihydrite, in most of cases spectra are interpreted as superpositions of signals originated from two octahedral sites,[41,44,45] however, contribution from tetrahedral site has not been excluded either.[46]

In previous studies on formation of xero- and aerogels formation of ferrihydrite,[19] goethite,[20] akagenite[21] were likewise reported. In all the mentioned regular structures (except β-FeOOH, akagenite) mostly one type of coordination is available for iron, *i.e.* one pair of δ, Δ values should describe the obtained Mössbauer spectra (in akagenite two types of sites exist[27]). In contrast to these expectations, three doublets are necessary to obtain acceptable fits for our samples (Table 2). As for the number of necessary doublets the same conclusion is reported in ref. 34. Additionally, size effect of particles should also be taken into account. In the case of a regular iron oxide, hematite, it has been known since long time that the value of quadrupole splitting explicitly depends on the size of particles.[47] Similar behaviour of oxyhydroxide particles of different size may result in spectra composed of components displaying various quadrupole splittings.

Evaluating the data of Table 2 in more detail three groups of Fe^{3+} sites can be separated by considering the δ values ($0.2 < Fe^{3+}(1) < \sim 0.33 < Fe^{3+}(2) < \sim 0.52 < Fe^{3+}(3) < 0.66$ mm s^{-1}, respectively). The gap between these intervals is significant, thus probably different chemical environments should be assigned to the different δ values. The first region (0.2–0.33 mm s^{-1}) may characterize tetrahedral sites, the second interval (0.33–0.52 mm s^{-1}) can be assigned probably to the octahedral sites. The δ value for the third interval (0.52–0.66) is rather high – this component may probably indicate some incomplete structure, *e.g.* inclusion either of chloride or solvent molecules. In particular chloride may promote stabilisation of oxyhydroxides.[27,48] In correspondence, presence of chlorine in significant amounts is revealed in correspondence with combustion measurements of samples prepared in DMSO media (Table 4) and EEL spectroscopy of X-GLY sample (Fig. 8). Chlorine can be present either in form of chloride ions, or retained epichlorohydrin, 3-chloro-propane-1,2-diol or even 1,2-dichloropropanol can be formed by the addition of chloride to protonated epichlorohydrin as described in ref. 21.

Primary formation of ferrihydrite can also be proven from our XRD measurements, too. XRD patterns reveal dominant presence of 2-line ferrihydrite in each of characterized samples (Fig. 3). Additionally, small contribution from goethite could also be detected in xerogel samples formed in DMSO media (Fig. 3c and d). Data are in good correspondence with results of recent X-ray scattering studies.[26]

Additional structural supporting information can be extracted from HRTEM data as well. SAED rings and HRTEM images of DMSO–water aerogel sample display rather large lattice constant ($\approx$1 nm). This value is in good correspondence with the 0.9 nm value reported for ferrihydrite in *c* direction of the hexagonal unit cell.[49] FFT patterns of aerogel samples exhibit diffraction rings at 0.21, 0.25 and 0.30 nm (Fig. 5). The very same values are reported for ferrihydrite in a recent report, too.[26] However, the rings in our samples are less sharp, and diffraction spots can hardly be distinguished even at the best resolution. Thus, considering the results obtained with various methods, dominating presence of imperfect ferrihydrite particles can be suggested in our samples.

As for transformations of aerogels due to modest temperature treatments one of our samples (A-(DMSO + H_2O)) was characterized after evacuation carried out at 260 °C. Adsorption measurements revealed significant textural changes. However, characteristic properties of aerogels were retained (high specific surface area, large pore volume *etc.*, Fig. 2 and Table 1). XRD measurements attest also for preservation of the original structure, the diffraction patterns of the original and evacuated samples are similar (Fig. 3a and b). Mössbauer spectra reveal also certain changes, early stages of magnetite formation can be traced from appearance of a minor Fe^{2+} component in the corresponding spectrum (Fig. 6h), however it is clearly different from spectra of regular magnetite. Furthermore the product can be magnetized with a permanent magnet. Similar behaviour upon a moderate heat treatment has also been reported in several communications.[6–8,43,50]

Conclusions

Aerogels and xerogels were prepared by hydrolysis of $FeCl_3 \cdot 6H_2O$ in organic solvents by using water molecules accessible solely from crystals of the starting iron salt. The process was

promoted with addition of a proton scavanger, epichlorohydrin. High surface area and low density aerogel products were obtained by supercritical CO_2 extraction of solvents. Xerogel samples are tight, compact and transparent substances.

Appearance of transient components in the early stages of formation of oxyhydroxo complexes can be revealed by Mössbauer spectroscopy in frozen solutions. In particular, stepwise exchange of ligands was clearly demonstrated in DMFA solvent. Simultaneously, dramatic increase of the probability of Mössbauer effect was also observed with the progress of hydrolysis. The process was slightly faster in DMSO, and even faster in ethylene glycol.

The loose structure of aerogels is reflected in their Mössbauer spectra: low response factor and asymmetric spectra are observed. The response factor dramatically increases upon compression, and the spectra display symmetric shape. On the other side high response factor and symmetric spectra are characteristic for frozen gel or dried xerogel samples. The formed nanoparticles are separated in both the aero- and xerogels, since magnetic ordering has not been detected in any of the Mössbauer spectra.

The xero- and aerogels are probably composed of imperfect ferrihydrite particles due to the low (ambient) temperature of synthesis. Their typical sizes are in the 4–8 nm region. SAED and FFT images are in good correspondence with results of other structural studies. In accordance, three characteristic coordination environments could be distinguished in the Mössbauer spectra, two of them reflect the structure of ferrihydrite, the third may correspond to certain imperfect iron siting, most probably in relation with presence of chloride.

Acknowledgements

The work was supported by the TÁMOP-4.2.2.A-11/1/KONV-2012-0036 project. The project is co-financed by the European Union and the European Social Fund. The authors are thankful to Lajos Daróczi (Dept. of Solid State Physics, University of Debrecen) for preparing the SEM micrographs.

References

1 A. S. Poyraz, C.-H. Kuo, S. Biswas, C. K. King'ondu and S. L. Suib, *Nat. Commun.*, 2013, **4**, 2952.
2 F. Jiao, A. Harrison, J.-C. Jumas, A. V. Chadwick, W. Kockelmann and P. G. Bruce, *Angew. Chem., Int. Ed.*, 2004, **43**, 5958.
3 D. N. Srivastava, N. Perkas, A. Gedanken and I. Felner, *J. Phys. Chem. B*, 2002, **106**, 1878–1883.
4 A. Du, B. Zhou, Z. Zhang and J. Shen, *Materials*, 2013, **6**, 941–968.
5 I. Lázár and I. Fábián, Patent WO 2013/061104, 2013.
6 J. Xu, H. Yang, W. Fu, K. Du, Y. Sui, J. Chen, Y. Zeng, M. Li and G. Zou, *J. Magn. Magn. Mater.*, 2007, **309**, 307–311.
7 E. E. Carpenter, J. W. Long, D. R. Rolison, M. S. Logan, K. Pettigrew, R. M. Stroud, L. Theil Kuhn, B. Rosendahl Hansen and S. Mørup, *J. Appl. Phys.*, 2006, **99**, 08N7117.
8 J. W. Long, M. S. Logan, C. P. Rhodes, E. E. Carpenter, R. M. Stroud and D. R. Rolison, *J. Am. Chem. Soc.*, 2004, **126**, 16879–16889.
9 P. Fabrizioli, T. Bürgi, M. Burgener, S. van Doorslaer and A. Baiker, *J. Mater. Chem.*, 2002, **12**, 619–630.
10 S. Bali, F. E. Huggins, G. P. Huffman, R. D. Ernst, R. J. Pugmire and E. M. Eyring, *Energy Fuels*, 2009, **23**, 14–18.
11 M.-S. Shin, J.-K. Kim, J.-W. Kim, C. A. Mendes Moraes, H.-S. Kim and K.-K. Koo, *J. Ind. Eng. Chem.*, 2012, **18**, 1768–1773.
12 S.-O. Kim, W. C. Lee, H. G. Choo, B.-T. Lee, P.-K. Lee and S. H. Choi, *Environ. Technol.*, 2014, **35**, 251–261.
13 F. Gschwind and M. Jansen, *Z. Kristallogr.*, 2014, **229**, 5–6.
14 I. G. Gusakovskaya, T. I. Larkina, V. I. Ponomarev and L. O. Atovmyan, *J. Struct. Chem.*, 1982, **23**, 864–869.
15 I. P. Lavrentiev, L. G. Korableva, E. A. Lavrentieva, G. A. Nifontova, M. L. Khidekel, I. G. Gusakovskaya, T. I. Larkina, L. D. Arutyuinian, O. S. Filipenko, V. I. Ponomarev and L. O. Atovmyan, *Transition Met. Chem.*, 1980, **5**, 193–200.
16 V. T. Yilmaz and Y. Topcu, *Termochim. Acta*, 1997, **307**, 143–147.
17 A. Asan, M. Andac and I. Isildak, *Anal. Sci.*, 2003, **19**, 1033–1036.
18 U. N. Tripathi, M. Afshan Siddiqui, S. Ahmad and K. Singh, *J. Coord. Chem.*, 2010, **63**, 894–905.
19 A. E. Gash, T. M. Tillotson, J. H. Satcher Jr, J. F. Poco, L. W. Hrubesh and R. L. Simpson, *Chem. Mater.*, 2001, **13**, 999–1007.
20 L. Durães, B. F. O. Costa, J. Vasques, J. Campos and A. Portugal, *Mater. Lett.*, 2005, **59**, 859–863.
21 A. E. Gash, J. H. Satcher Jr and R. L. Simpson, *Chem. Mater.*, 2003, **15**, 3265–3278.
22 S. Bali, G. C. Turpin, R. D. Ernst, R. J. Pugmire, V. Singh, M. S. Seehra and E. M. Eyring, *Energy Fuels*, 2008, **22**, 1439–1443.
23 M. V. Twigg and J. Burgess, in *Comprehensive Coordination Chemistry II*, Elsevier, vol. 5, 2003, pp. 403–553.
24 G. Lente and I. Fábián, *Inorg. Chem.*, 1999, **38**, 603–605.
25 J. Livage, M. Henry and C. Sanchez, *Prog. Solid State Chem.*, 1988, **18**, 259–341.
26 F. M. Michel, L. Ehm, G. Liu, W. Q. Han, S. M. Antao, P. J. Chupas, P. L. Lee, K. Knorr, H. Eulert, J. Kim, C. P. Grey, A. J. Celestian, O. J. Gillow, M. A. A. Schoonen, D. R. Strongin and J. B. Parise, *Chem. Mater.*, 2007, **19**, 1489–1496.
27 R. M. Cornell and U. Schwertmann, *The Iron Oxides*, Weinheim, 1996.
28 E. Murad and J. H. Johnston, in *Mössbauer Spectroscopy Applied to Inorganic Chemistry*, ed. G. J. Long, Plenum Press, vol. 2, 1987, pp. 507–582.
29 M. D. Lind, *J. Chem. Phys.*, 1967, **47**, 990–993.
30 N. Thrane and G. Trumpy, *Phys. Rev. B*, 1970, **1**, 153–155.
31 J. H. Johnston and D. G. Lewis, in *Industrial Applications of Mössbauer Effect*, ed G. J. Long and J. G. Stevens, Plenum, 1986, pp. 565–583.

32 A. Vértes, The chemical structure of liquid solutions studied by Mössbauer spectroscopy, in *Mössbauer Spectroscopy of Frozen Solutions*, ed. A. Vértes and D. L. Nagy, Akadémiai, Budapest, 1990.
33 K. Burger, *Solvation, ionic and complex formation reaction in non-aqueous solvents. Studies in Analytical Chemistry*, Elsevier–Akadémiai, Budapest, 1983, vol. 6.
34 F. E. Huggins, S. Bali, G. P. Huffman and E. M. Eyring, *Spectrochim. Acta, Part A*, 2010, **76**, 74–83.
35 A. Vértes, L. Korecz and K. Burger, *Mössbauer spectroscopy*, Akadémiai Kiadó, Budapest, 1979.
36 R. V. Parish, in *Mössbauer Spectroscopy Applied to Inorganic Chemistry*, Plenum, 1984, vol. 1, pp. 527–575.
37 K. Lázár, K. Matusek, J. Mink, S. Dobos, L. Guczi, A. Vizi-Orosz, L. Markó and W. M. Reiff, *J. Catal.*, 1984, **87**, 163–178.
38 T. Belgya and K. Lázár, *Hyperfine Interact.*, 2006, **167**, 875–879.
39 S. Brunauer, P. H. Emmett and E. Teller, *J. Am. Chem. Soc.*, 1938, **60**, 309–319.
40 P. Bussière and P. Vergnon, *J. Phys. I*, 1980, **41**, C1-147–C1-148.
41 M. Blume, *Phys. Rev. Lett.*, 1967, **18**, 305–308.
42 Y. Guyodo, S. K. Banerjee, R. L. Penn, D. Burleson, T. S. Berquo, T. Seda and P. Solheid, *Phys. Earth Planet. Inter.*, 2006, **154**, 222–233.
43 V. Klimas, K. Mažeika, V. Jasulaitiene and A. Jagminas, *J. Fluorine Chem.*, 2015, **170**, 1–9.
44 Q. A. Pankhurst and R. J. Pollard, *Clays Clay Miner.*, 1992, **40**, 268–272.
45 E. Murad, *J. Magn. Magn. Mater.*, 1988, **74**, 153–157.
46 C. M. Cardile, *Clays Clay Miner.*, 1988, **36**, 537–539.
47 W. Kündig, H. Bömmel, G. Constabaris and R. H. Lindquist, *Phys. Rev.*, 1966, **142**, 327–333.
48 A. S. Campbell, U. Schwertmann and P. A. Campbell, *Clay Miner.*, 1997, **32**, 615–622.
49 F. M. Michel, L. Ehm, S. M. Antao, P. L. Lee, P. J. Chupas, G. Liu, D. R. Strongin, M. A. A. Schoonen, B. L. Phillips and J. B. Parise, *Science*, 2007, **316**, 1726–1729.
50 Ö. Özdemir and D. J. Dunlop, *Earth Planet. Sci. Lett.*, 2000, **177**, 59–67.